

EUROPEAN ORGANISATION FOR NUCLEAR RESEARCH (CERN)



Submitted to: Phys. Rev. Lett.



CERN-EP-2022-229
3rd February 2023

Observation of single-top-quark production in association with a photon using the ATLAS detector

The ATLAS Collaboration

This Letter reports the observation of single top quarks produced together with a photon using 139 fb^{-1} of 13 TeV proton–proton collision data collected with the ATLAS detector at the Large Hadron Collider. The analysis uses the presence of a forward jet, characteristic of t -channel production, and separates the signal from the background with neural networks. Requiring a photon with transverse momentum larger than 20 GeV and within the detector acceptance, the fiducial cross section is measured to be $688 \pm 23 \text{ (stat.)}^{+75}_{-71} \text{ (syst.) fb}$, to be compared with the Standard Model prediction of $515^{+36}_{-42} \text{ fb}$ at next-to-leading order in QCD.

Measurements of rare associated-production processes of the top quark (t) are fundamental in probing the top quark's electroweak couplings. While pair production ($t\bar{t}$) has been observed in association with a Higgs boson [1, 2], W boson [3], Z boson [3, 4] or photon (γ) [5], single-top-quark production has so far only been observed in association with a Z [6, 7] or W boson [8, 9]. These processes play a crucial role in constraining nonresonant contributions from physics beyond the Standard Model (SM), parameterized in the framework of the SM effective field theory (EFT) [10–14]. This Letter reports the observation of single-top-quark production in association with a photon in the dominant t -channel mode with the ATLAS detector [15] at the Large Hadron Collider (LHC). The full 13 TeV proton–proton (pp) dataset is used, corresponding to an integrated luminosity of 139 fb^{-1} [16]. The CMS Collaboration previously reported evidence for this process using 35.9 fb^{-1} of pp data collected at 13 TeV [17].

In single-top-quark production, a photon can be radiated from any of the charged particles in the initial and final states, but the radiation before the top-quark decay is of particular interest. This process is sensitive to the top–photon coupling and is called $tq\gamma$ in the following, where q stands for the additional quark produced in the t -channel. An example Feynman diagram is shown in Figure 1, where the top quark decays semileptonically ($t \rightarrow \ell\nu b$). The signature of this process consists of a photon, an electron or muon (ℓ), missing transverse momentum (E_T^{miss}) from the neutrino, a b -jet from the top-quark decay, and a forward jet characteristic of t -channel production. The latter jet, from the second b -quark, is often not b -tagged because of its low transverse momentum and forward direction. Hadronic top-quark decays are not considered as signal in this analysis. The photon can also be radiated from the top quark's charged decay products, called the $t \rightarrow \ell\nu b\gamma$ q process.

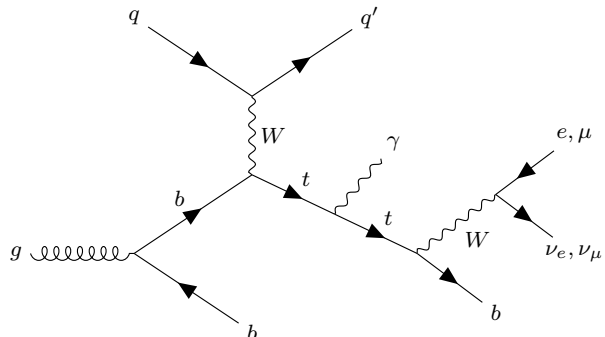


Figure 1: Representative Feynman diagram at leading order in α_s for $tq\gamma$ production with semileptonic top-quark decay.

The cross section for $tq\gamma$ production is measured in a fiducial phase space at parton level, excluding the contribution from $t \rightarrow \ell\nu b\gamma$ q . The parton-level measurement can be compared with fixed-order predictions for the $tq\gamma$ cross section. In addition, a fiducial cross section at particle level is measured, including both the $tq\gamma$ and $t \rightarrow \ell\nu b\gamma$ q processes.

The ATLAS detector is a multipurpose particle physics detector with cylindrical geometry¹. It consists of an inner tracker (ID) surrounded by a superconducting solenoid, sampling electromagnetic (EM) and hadronic calorimeters, and a muon spectrometer (MS) with three toroidal superconducting magnets with eight coils

¹ ATLAS uses a right-handed coordinate system with its origin at the nominal interaction point (IP) in the center of the detector and the z -axis along the beam pipe. The x -axis points from the IP to the center of the LHC ring, and the y -axis points upwards. Cylindrical coordinates (r, ϕ) are used in the transverse plane, ϕ being the azimuthal angle around the z -axis. The pseudorapidity is defined in terms of the polar angle θ as $\eta = -\ln \tan(\theta/2)$. Angular distance is measured in units of $\Delta R \equiv \sqrt{(\Delta\eta)^2 + (\Delta\phi)^2}$.

each. A two-level trigger system is used to select events for storage. Events used in this analysis were selected online by sets of single-electron or single-muon triggers with their lowest transverse-momentum (p_T) thresholds being 20–26 GeV, depending on the data-taking year [18–20]. An extensive software suite [21] is used in data simulation, in the reconstruction and analysis of real and simulated data, in detector operations, and in the trigger and data acquisition systems of the experiment.

The proton interaction vertex with the highest p_T^2 sum of associated ID tracks is selected as the primary vertex (PV). Electrons and photons are reconstructed from energy deposits in the EM calorimeter [22]. Electrons have an associated ID track [23], while photons either have no track or have tracks that are consistent with arising from a conversion ($\gamma \rightarrow e^+e^-$). Electrons (photons) must be isolated from surrounding ID tracks and energy deposits in the calorimeters [24], fulfill the “tight” identification criteria [22], have $p_T > 27$ GeV (20 GeV) and satisfy $|\eta| < 2.47$ (2.37), excluding $1.37 < |\eta| < 1.52$. Muons are reconstructed from MS [25] and ID tracks, must fulfill the “medium” identification criteria [25], $p_T > 27$ GeV, $|\eta| < 2.5$, and be isolated [24]. Electrons and muons must be matched to the PV. Jets are reconstructed from particle-flow objects [26] using the anti- k_t algorithm [27, 28] with $R = 0.4$. Jets must fulfill $p_T > 25$ GeV and $|\eta| < 4.5$. Jets with $p_T < 60$ GeV and $|\eta| < 2.5$ must fulfill the “jet vertex tagger” requirements to reduce the impact of additional jets from overlapping collisions in the same or neighboring bunch crossings (pileup) [29]. Overlaps between reconstructed electrons, muons, photons and jets are resolved [24] so as to avoid double counting of detector signatures and to ensure a minimum distance between objects. Jets within $|\eta| < 2.5$ are checked with the “DL1r” algorithm [30–32] to determine whether they should be b -tagged or not, based on secondary-vertex and impact-parameter information from ID tracks. The magnitude of the E_T^{miss} [33] is calculated from the negative vector sum of the p_T of PV-associated reconstructed objects. The contribution from tracks that are associated with the PV but not with a reconstructed object is also accounted for.

Two signal regions (SR) are defined, based on the presence or absence of a forward jet (fj) in the event. In both SRs, the presence of one photon, one electron or muon matched to a trigger object, one tight b -tagged jet, no additional loose b -tagged jets and $E_T^{\text{miss}} > 30$ GeV is required. In addition, the 0fj SR (≥ 1 fj SR) must contain no (at least one) forward jet with $2.5 < |\eta| < 4.5$. The tight and loose operating points of DL1r correspond to b -tagging efficiencies of 70% and 85%, estimated in $t\bar{t}$ Monte Carlo (MC) simulations. In both SRs, the electron–photon invariant mass must be outside the range 80–100 GeV to suppress the $Z \rightarrow ee$ contribution with an electron misidentified as a photon.

A fiducial phase space is defined at parton level, i.e. before parton showering and hadronization, requiring at least one photon with $p_T > 20$ GeV and $|\eta| < 2.37$ that must be Frixione-isolated [34] with a chosen isolation radius of $\Delta R = 0.2$. Following Ref. [35], the fixed-order SM fiducial cross section times branching ratio² $\mathcal{B}(t \rightarrow \ell v b)$ is calculated with **MADGRAPH5_AMC@NLO** [36] at next-to-leading order (NLO) in QCD as $\sigma_{tq\gamma} \times \mathcal{B}(t \rightarrow \ell v b) = 515^{+36}_{-42}$ fb. The cross-section calculation uses the five-flavor scheme, with b -quarks included in the proton. Renormalization and factorization scales as well as the set of parton distribution functions (PDF) are chosen as in Ref. [35]. The uncertainties are estimated from scale and PDF variations and a comparison with the corresponding calculation in the four-flavor scheme (no third-generation quarks in the proton) [35, 37].

An additional fiducial phase space is defined at particle level, close to the SR definitions, requiring one electron or muon with $p_T > 25$ GeV and $|\eta| < 2.5$, at least one photon with $p_T > 20$ GeV and $|\eta| < 2.37$, at least one b -tagged jet with $p_T > 25$ GeV and $|\eta| < 2.5$, and at least one neutrino not from a hadron decay. The particle-level objects are photons not from a hadron decay, prompt electrons and muons “dressed” by adding nearby ($\Delta R < 0.1$) photons, and anti- k_t , $R = 0.4$ jets built from stable particles (lifetime

² The branching ratio for $t \rightarrow \ell v b$ is set to 32.46%, consistent with the value in the signal MC samples.

larger than 30 ps) and τ -leptons, excluding neutrinos and prompt dressed muons. Jets are b -tagged using ghost-matched [38] b -hadrons with $p_T > 5$ GeV. Jets within $\Delta R = 0.4$ of a photon are removed if the p_T of charged particles within $\Delta R = 0.3$ of the photon is less than 10% of its p_T . Jets within $\Delta R = 0.4$ of a lepton are removed. Events where a photon is close ($\Delta R < 0.4$) to a lepton or a surviving jet are removed. The SM fiducial cross section at particle level times branching ratio is calculated at NLO in QCD using the signal samples for $tq\gamma$ and $t (\rightarrow \ell v b \gamma) q$ defined below: $\sigma_{tq\gamma} \times \mathcal{B}(t \rightarrow \ell v b) + \sigma_{t (\rightarrow \ell v b \gamma) q} = 217^{+27}_{-15}$ fb. The uncertainty includes PDF and scale variations, uncertainties in the parton shower model, the choice of matrix-element generator, the modeling of initial- and final-state radiation and a 20% uncertainty in the $t (\rightarrow \ell v b \gamma) q$ process normalization (cf. the “end matter” addendum). The $t (\rightarrow \ell v b \gamma) q$ process makes up $\approx 20\%$ of the events in the fiducial region.

The most important background processes with prompt photons are $t\bar{t}\gamma$ and $W\gamma$ production. Their contribution to the SRs is estimated using MC simulations, normalized to data in dedicated control regions (CRs) enriched in $t\bar{t}\gamma$ and $W\gamma$ events. The CRs are inclusive in forward jets and the same selection criteria as for the SRs are used, except for the b -tagging requirements. In the $t\bar{t}\gamma$ CR, an additional loose b -tagged jet must be present. In the $W\gamma$ CR, there must be at least one loose b -tagged jet and no tight b -tagged jets. Other important backgrounds arise from electrons (hadrons) that are misidentified as photons, denoted by $e \rightarrow \gamma$ ($h \rightarrow \gamma$). The modeling of these $e \rightarrow \gamma$ and $h \rightarrow \gamma$ fake-photon background contributions in MC simulations is adjusted using data-driven methods. According to MC simulations, the signal fraction (“ $tq\gamma$ ” plus “ $t (\rightarrow \ell v b \gamma) q$ ”) in the 0fj (≥ 1 fj) SR is 5% (10%) and the main backgrounds are $t\bar{t}\gamma$ with 29% (34%), $e \rightarrow \gamma$ fake-photon events with 24% (25%), $W\gamma$ +jets with 20% (12%) and $h \rightarrow \gamma$ fake events with 7% (7%). Smaller backgrounds originate from other processes with prompt photons.

Signal and most background processes are estimated with MC simulations, which include pileup effects. The full GEANT4-based [39] ATLAS detector simulation is used [40] with corrections applied for the different reconstructed objects [22, 25, 29, 30, 33, 41].

The $tq\gamma$ process was simulated in the four-flavor scheme at NLO in QCD with **MADGRAPH5_AMC@NLO** using the NNPDF3.0 [42] PDF set and **MADSPIN** [43] for $t \rightarrow Wb \rightarrow \ell v b$ decay. Photons must be Frixione-isolated and have $p_T > 10$ GeV and $|\eta| < 5.0$. Renormalization and factorization scales were set to $\frac{1}{2} \sum_i \sqrt{m_i^2 + p_{T,i}^2}$, where the sum is over all final-state particles after the top-quark decay. **PYTHIA 8** [44] was used for parton showering and hadronization. **PYTHIA 8** always used the leading-order (LO) NNPDF2.3 PDF set [45], the A14 tune [46], and **EVTGEN** [47]. The $t (\rightarrow \ell v b \gamma) q$ process was simulated via single-top-quark production in the t -channel (without photon radiation) using **POWHEG** [48] in the four-flavor scheme at NLO with the NNPDF3.0 PDF set, interfaced to **PYTHIA 8** and **MADSPIN** for the semileptonic top-quark decay. Photon radiation in the decay was treated by the parton-shower simulation. Initially, the $tq\gamma$ process is normalized to the cross section at NLO in QCD obtained with **MADGRAPH5_AMC@NLO** and the same settings used for the sample production, and the $t (\rightarrow \ell v b \gamma) q$ process is normalized to the production cross section at NLO in QCD [49, 50]. The overlap between the $tq\gamma$ and $t (\rightarrow \ell v b \gamma) q$ samples is removed using kinematic information about the generated particles (cf. end matter).

Background contributions are estimated using MC simulations, except for a small contribution with fake leptons, i.e. other objects that are misidentified as electron or muon, estimated from data using the asymptotic matrix method with loosened lepton criteria [51, 52]. The background MC samples use the same setups as in Ref. [24] and include the following processes (cf. end matter): $t\bar{t}\gamma$, $t\bar{t}$ with radiative decay ($t \rightarrow \ell v b \gamma$ and $t \rightarrow q\bar{q}'b\gamma$), $W\gamma/Z\gamma$ +jets, $t\bar{t}$, single top quark, W/Z +jets and diboson production.

The MC predictions for background processes with $e \rightarrow \gamma$ fakes, most notably dileptonic $t\bar{t}$ events, are corrected by comparing the $e \rightarrow \gamma$ probability in data and MC simulation using $Z \rightarrow e^+e^-$ events [53].

Events with $E_T^{\text{miss}} < 30 \text{ GeV}$ and no b -tagged jet are selected if the invariant mass of either an e^+e^- pair or an $e\gamma$ pair is close to the Z -boson mass, where the photon in the latter case is likely from $e \rightarrow \gamma$. Data-to-MC corrections are derived as functions of the photon η and the different types of photon reconstruction [22]. No strong dependence of the corrections on the photon p_T is found. The corrections are validated by comparing data with the prediction in a region with $E_T^{\text{miss}} < 30 \text{ GeV}$ and at least one b -tagged jet.

The MC predictions for background processes with $h \rightarrow \gamma$ fakes, mostly lepton+jets $t\bar{t}$ events, are also corrected using data [53]. Selections with partially inverted photon-identification and/or inverted photon-isolation criteria are used, respectively, to define regions that are kinematically close to the analysis regions but enriched in events with $h \rightarrow \gamma$. Considering the low correlation between the identification and isolation criteria, the ABCD method (see for example Ref. [54]) is used to estimate the number of $h \rightarrow \gamma$ events in the analysis regions. This residual small correlation is taken from MC simulations and is corrected for in the estimate. The $h \rightarrow \gamma$ rate estimate is performed in two bins of photon p_T and as a function of photon reconstruction types and η , and is used to correct the overall normalization of the contribution from $h \rightarrow \gamma$ events.

Uncertainties in the photon identification [22, 55] and isolation efficiencies [22] are considered, as are those in the electron and muon trigger, reconstruction, identification and isolation efficiencies [22, 56, 57]; the photon and electron energy [22] and muon momentum scale and resolution [57]; the jet pileup rejection [29], and jet energy scale [41, 58], resolution [41] and b -tagging efficiency [30, 31, 59]; and the E_T^{miss} reconstruction [33].

Uncertainties in the inclusive cross sections and in the modeling (scale variations, comparisons of generator setups, etc.) of the different processes are considered (cf. end matter). Since the analysis includes CRs for the $t\bar{t}\gamma$ and $W\gamma$ +jets processes, their normalization is estimated directly from data.

Uncertainties in the $e \rightarrow \gamma$ corrections are estimated by varying the background contributions, the Z -boson MC modeling, the Z -boson mass range and the photon energy scale. Uncertainties in the $h \rightarrow \gamma$ corrections originate from the statistical uncertainties, the limited number of MC events, contributions from non- $h \rightarrow \gamma$ events, and variations of the correlation between the inverted identification and isolation criteria.

Neural networks (NNs) are trained to separate the signal from the background in the SRs. Keras [60] with the TensorFlow [61] backend is used with binary cross-entropy as the loss function. The NN output nodes use a sigmoid activation function. In the 0fj and ≥ 1 fj SRs, 12 and 15 input variables are used, respectively. These comprise the p_T , η and ϕ of the photon, the lepton, the b -tagged jet and the highest- p_T forward jet, kinematic combinations of these objects and the E_T^{miss} (scalar p_T sum, invariant and transverse masses), as well as the b -tagging properties of the b -tagged jet [30]. The top quark is reconstructed from the b -tagged jet, the lepton and the E_T^{miss} . The top-quark mass is the NN input variable giving the largest separation in both SRs as it separates $tq\gamma$ from backgrounds without a top quark, top-quark events with $t \rightarrow \ell\nu b\gamma$ as well as top-quark pair production where the chosen objects are less likely associated to the same top-quark decay. Figure 2 shows this variable in the $W\gamma$ CR as an example, illustrating that the data are described by the MC simulation within the uncertainties.

To test for the presence of $tq\gamma$ production and measure the signal cross sections, a profile-likelihood fit using asymptotic formulae [62] is performed simultaneously in the SRs and CRs with systematic uncertainties treated as nuisance parameters. The uncertainty due to the limited number of MC events is included [63]. In the 0fj (≥ 1 fj) SRs, the 0fj (≥ 1 fj) NN output distributions are used in the fit. In the $t\bar{t}\gamma$ CR, the 0fj (≥ 1 fj) NN output is used for events with no (at least one) forward jet, and the inclusive event yield is used in the $W\gamma$ CR. The $t\bar{t}\gamma$ and $W\gamma$ +jets normalizations are free parameters of the fit. The result of the fit is shown in Figure 3. The predicted sum of all backgrounds is not compatible with the data. The observed (expected)

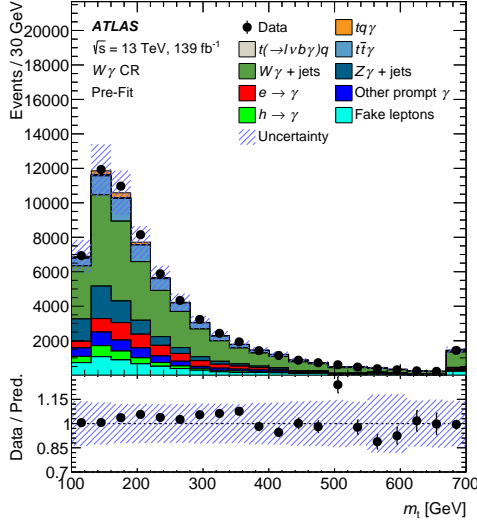


Figure 2: Distribution of the reconstructed top-quark mass in the $W\gamma$ CR before the profile-likelihood fit. The hashed band represents the uncertainties and the first and last bins include the underflow and overflow.

significance of the $tq\gamma$ signal is 9.3σ (6.8σ). The fitted $t\bar{t}\gamma$ and $W\gamma$ +jets normalizations are consistent with the nominal prediction within the uncertainties of $^{+14\%}_{-13\%}$ and $^{+20\%}_{-17\%}$.

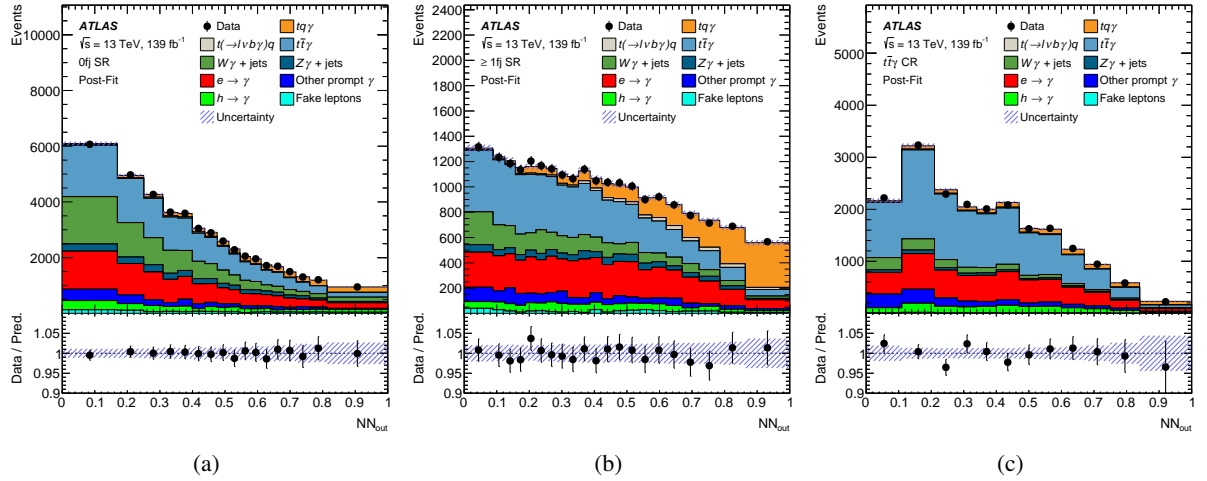


Figure 3: Distributions of the NN outputs in (a) the 0fj SR, (b) the ≥ 1 fj SR and (c) the $t\bar{t}\gamma$ CR in data and the expected contribution of the signal and background processes after the profile-likelihood fit. The hashed band represents the uncertainties in the SM prediction.

The measured fiducial parton-level cross section is $\sigma_{tq\gamma} \times \mathcal{B}(t \rightarrow \ell\nu b) = 688 \pm 23$ (stat.) $^{+75}_{-71}$ (syst.) fb. The measured fiducial particle-level cross section is $\sigma_{tq\gamma} \times \mathcal{B}(t \rightarrow \ell\nu b) + \sigma_{t(\rightarrow \ell\nu b\gamma)q} = 303 \pm 9$ (stat.) $^{+33}_{-32}$ (syst.) fb. Both phase-space definitions require the photon p_T to be at least 20 GeV. The main sources of systematic uncertainty in the parton-level (particle-level) measurement are the modeling of $t\bar{t}\gamma$ production with $\pm 5.5\%$ ($\pm 5.5\%$), the limited number of MC events for the background processes with $\pm 3.5\%$ ($\pm 3.6\%$) and for the $tq\gamma$ process with $\pm 3.3\%$ ($\pm 3.0\%$), and the modeling of the $t(\rightarrow \ell\nu b\gamma)q$

process with $\pm 1.9\%$ ($\pm 3.3\%$) and of the $t\bar{t}$ process with $\pm 2.4\%$ ($\pm 2.3\%$). The uncertainty in the modeling of the $t \rightarrow \ell\nu b\gamma$ q process has a larger impact on the particle-level measurement, because in the parton-level measurement the $t \rightarrow \ell\nu b\gamma$ q contribution is fixed to the SM expectation within its uncertainties. The measured fiducial cross sections at parton (particle) level are compatible with the SM predictions at NLO in α_s of 515^{+36}_{-42} fb (217^{+27}_{-15} fb) within 2.1 (2.0) standard deviations. The 30%–40% higher measured cross sections are consistent with the results of the CMS measurement [17], which yielded 1.42 ± 0.43 times the SM prediction in a slightly different fiducial phase space. Corrections at approximate next-to-next-to-leading order (NNLO) in a similar phase space were calculated to 5.1% [64]. In conclusion, this work adds the associated production of a single top quark and photon to the list of experimentally verified rare top-quark production processes [1–9].

End matter

This end matter contains additional information about signal and background MC samples and their systematic uncertainties.

In order to remove the overlap between the $tq\gamma$ and $t(\rightarrow \ell v b\gamma) q$ samples, events from the $t(\rightarrow \ell v b\gamma) q$ sample are kept when the hypothesis of a radiative-decay photon better approximates the true W -boson or top-quark mass, i.e. either the $\ell v\gamma$ or the $\ell v b\gamma$ invariant mass is closer than the ℓv or $\ell v b$ invariant mass to the W -boson or top-quark mass, respectively. The uncertainty associated with this procedure in the prediction of the fiducial cross section at particle level is conservatively estimated to be 20%, based on $tq\gamma$ events that are falsely categorized as $t(\rightarrow \ell v b\gamma) q$.

The background MC samples include the following production processes: $t\bar{t}\gamma$ (NLO), $t\bar{t}$ with radiative decay (LO), $W\gamma/Z\gamma$ +jets (NLO for up to one additional parton, LO for up to three) [65–75], $t\bar{t}$ [76–79], single top quark [48, 80], W/Z +jets (NLO for up to two additional partons, LO for up to four) and diboson (NLO for up to one additional parton, LO for up to three). The overlap between samples with photons generated in the matrix element and those with photons from the parton shower is removed using generator-level information. The numbers of events from several MC samples are normalized to cross sections calculated to higher orders in α_s : NNLO plus next-to-next-to-leading-logarithm precision for $t\bar{t}$ production [81–87], NNLO precision for W +jets and Z +jets production [88] and NLO (NNLO) precision for single-top-quark production in the t - and s -channel [49, 50] (tW -channel [89]). For $t\bar{t}$ production with radiative decay, a LO-to-NLO correction factor of 1.67 is determined by subtracting the NLO `MADGRAPH5_AMC@NLO` prediction for the $t\bar{t}\gamma$ process from an NLO calculation of the full process [90].

The uncertainties in the inclusive cross sections amount to 6% for $t\bar{t}$ [45, 87, 91–93], 5.3% for single-top-quark production [89, 94, 95], 5% for W +jets and Z +jets [96], 30% for $Z\gamma$ +jets and 50% for diboson production, mostly in association with b -jets. An additional uncertainty of 30% is assigned for the normalization of $W\gamma$ production in association with b -jets. The possible phase-space dependence of the LO-to-NLO correction factor for $t\bar{t}$ production with radiative decay is estimated by changing the correction factor from 1.67 to 1.97, motivated by the correction determined in Ref. [97]. A 30% uncertainty is assigned to the normalization of the $t(\rightarrow \ell v b\gamma) q$ process, conservatively taken to be of the order of the difference between the predicted $t(\rightarrow \ell v b\gamma) q$ event yields at LO and NLO. Uncertainties in the fake-lepton background arise from the uncertainties in the prompt-lepton subtraction in the matrix method and from a 50% normalization uncertainty. The uncertainty in the integrated luminosity is 1.7% [16]. The uncertainty in the simulation of pileup is estimated by varying the average expected number of interactions per bunch crossing by 3%.

Modeling uncertainties are evaluated as follows. Renormalization and factorization scales as well as PDFs are varied in the signal and background MC samples. The uncertainty from the choice of MC generator is estimated by comparing the nominal $t(\rightarrow \ell v b\gamma) q$, $t\bar{t}$ and tW samples with alternative samples generated with `MADGRAPH5_AMC@NLO` interfaced to `PYTHIA` 8. For the tW sample, the difference between the diagram-subtraction scheme and the nominal diagram-removal scheme [80] is used as an uncertainty. The uncertainty from the choice of parton-shower program is estimated by comparing the nominal signal, $t\bar{t}\gamma$, $t\bar{t}$ and tW samples with samples interfaced to `HERWIG` 7 [98, 99]. The $t\bar{t}$ sample is compared with a sample with the value of the h_{damp} parameter, controlling the p_T of the first gluon emission in the `POWHEG` generator, increased from $1.5 m_{\text{top}}$ to $3 m_{\text{top}}$ [100]. The uncertainty in the modeling of ISR/FSR is estimated by systematic variations in the A14 tune [46] in the signal, $t\bar{t}\gamma$ and $t\bar{t}$ samples. In addition, an uncertainty

in the $t \rightarrow \ell \nu b \gamma$ q sample is estimated by comparing the shapes predicted by the nominal sample with the shapes predicted by a LO sample with the decay $t \rightarrow \ell \nu b \gamma$ q simulated directly in the hard process with `MADGRAPH5_AMC@NLO` using the NNPDF2.3 PDF set and interfaced with `PYTHIA 8`.

References

- [1] ATLAS Collaboration, *Observation of Higgs boson production in association with a top quark pair at the LHC with the ATLAS detector*, *Phys. Lett. B* **784** (2018) 173, arXiv: [1806.00425 \[hep-ex\]](#).
- [2] CMS Collaboration, *Observation of $t\bar{t}H$ Production*, *Phys. Rev. Lett.* **120** (2018) 231801, arXiv: [1804.02610 \[hep-ex\]](#).
- [3] CMS Collaboration, *Measurement of the cross section for top quark pair production in association with a W or Z boson in proton–proton collisions at $\sqrt{s} = 13$ TeV*, *JHEP* **08** (2018) 011, arXiv: [1711.02547 \[hep-ex\]](#).
- [4] ATLAS Collaboration, *Measurement of the $t\bar{t}Z$ and $t\bar{t}W$ cross sections in proton–proton collisions at $\sqrt{s} = 13$ TeV with the ATLAS detector*, *Phys. Rev. D* **99** (2019) 072009, arXiv: [1901.03584 \[hep-ex\]](#).
- [5] ATLAS Collaboration, *Observation of top-quark pair production in association with a photon and measurement of the $t\bar{t}\gamma$ production cross section in pp collisions at $\sqrt{s} = 7$ TeV using the ATLAS detector*, *Phys. Rev. D* **91** (2015) 072007, arXiv: [1502.00586 \[hep-ex\]](#).
- [6] ATLAS Collaboration, *Observation of the associated production of a top quark and a Z boson in pp collisions at $\sqrt{s} = 13$ TeV with the ATLAS detector*, *JHEP* **07** (2020) 124, arXiv: [2002.07546 \[hep-ex\]](#).
- [7] CMS Collaboration, *Observation of Single Top Quark Production in Association with a Z Boson in Proton–Proton Collisions at $\sqrt{s} = 13$ TeV*, *Phys. Rev. Lett.* **122** (2019) 132003, arXiv: [1812.05900 \[hep-ex\]](#).
- [8] ATLAS Collaboration, *Measurement of the production cross-section of a single top quark in association with a W boson at 8 TeV with the ATLAS experiment*, *JHEP* **01** (2016) 064, arXiv: [1510.03752 \[hep-ex\]](#).
- [9] CMS Collaboration, *Observation of the Associated Production of a Single Top Quark and a W Boson in pp Collisions at $\sqrt{s} = 8$ TeV*, *Phys. Rev. Lett.* **112** (2014) 231802, arXiv: [1401.2942 \[hep-ex\]](#).
- [10] A. Buckley et al., *Constraining top quark effective theory in the LHC Run II era*, *JHEP* **04** (2016) 015, arXiv: [1512.03360 \[hep-ph\]](#).
- [11] N. P. Hartland et al., *A Monte Carlo global analysis of the Standard Model Effective Field Theory: the top quark sector*, *JHEP* **04** (2019) 100, arXiv: [1901.05965 \[hep-ph\]](#).
- [12] G. Durieux et al., *The electro-weak couplings of the top and bottom quarks — Global fit and future prospects*, *JHEP* **12** (2019) 98, [Erratum: *JHEP* **01**, 195 (2021)], arXiv: [1907.10619 \[hep-ph\]](#).
- [13] I. Brivio et al., *O new physics, where art thou? A global search in the top sector*, *JHEP* **02** (2020) 131, arXiv: [1910.03606 \[hep-ph\]](#).
- [14] V. Miralles et al., *The top quark electro-weak couplings after LHC Run 2*, *JHEP* **02** (2022) 032, arXiv: [2107.13917 \[hep-ph\]](#).
- [15] ATLAS Collaboration, *The ATLAS Experiment at the CERN Large Hadron Collider*, *JINST* **3** (2008) S08003.

- [16] ATLAS Collaboration, *Luminosity determination in pp collisions at $\sqrt{s} = 13$ TeV using the ATLAS detector at the LHC*, ATLAS-CONF-2019-021, 2019, URL: <https://cds.cern.ch/record/2677054>.
- [17] CMS Collaboration, *Evidence for the Associated Production of a Single Top Quark and a Photon in Proton–Proton Collisions at $\sqrt{s} = 13$ TeV*, *Phys. Rev. Lett.* **121** (2018) 221802, arXiv: [1808.02913 \[hep-ex\]](https://arxiv.org/abs/1808.02913).
- [18] ATLAS Collaboration, *Performance of the ATLAS trigger system in 2015*, *Eur. Phys. J. C* **77** (2017) 317, arXiv: [1611.09661 \[hep-ex\]](https://arxiv.org/abs/1611.09661).
- [19] ATLAS Collaboration, *Performance of electron and photon triggers in ATLAS during LHC Run 2*, *Eur. Phys. J. C* **80** (2020) 47, arXiv: [1909.00761 \[hep-ex\]](https://arxiv.org/abs/1909.00761).
- [20] ATLAS Collaboration, *Performance of the ATLAS muon triggers in Run 2*, *JINST* **15** (2020) P09015, arXiv: [2004.13447 \[hep-ex\]](https://arxiv.org/abs/2004.13447).
- [21] ATLAS Collaboration, *The ATLAS Collaboration Software and Firmware*, ATL-SOFT-PUB-2021-001, 2021, URL: <https://cds.cern.ch/record/2767187>.
- [22] ATLAS Collaboration, *Electron and photon performance measurements with the ATLAS detector using the 2015–2017 LHC proton–proton collision data*, *JINST* **14** (2019) P12006, arXiv: [1908.00005 \[hep-ex\]](https://arxiv.org/abs/1908.00005).
- [23] ATLAS Collaboration, *Performance of the ATLAS track reconstruction algorithms in dense environments in LHC Run 2*, *Eur. Phys. J. C* **77** (2017) 673, arXiv: [1704.07983 \[hep-ex\]](https://arxiv.org/abs/1704.07983).
- [24] ATLAS Collaboration, *Search for flavour-changing neutral-current couplings between the top quark and the photon with the ATLAS detector at $\sqrt{s} = 13$ TeV*, (2022), arXiv: [2205.02537 \[hep-ex\]](https://arxiv.org/abs/2205.02537).
- [25] ATLAS Collaboration, *Muon reconstruction and identification efficiency in ATLAS using the full Run 2 pp collision data set at $\sqrt{s} = 13$ TeV*, *Eur. Phys. J. C* **81** (2021) 578, arXiv: [2012.00578 \[hep-ex\]](https://arxiv.org/abs/2012.00578).
- [26] ATLAS Collaboration, *Jet reconstruction and performance using particle flow with the ATLAS Detector*, *Eur. Phys. J. C* **77** (2017) 466, arXiv: [1703.10485 \[hep-ex\]](https://arxiv.org/abs/1703.10485).
- [27] M. Cacciari, G. P. Salam and G. Soyez, *The anti- k_t jet clustering algorithm*, *JHEP* **04** (2008) 063, arXiv: [0802.1189 \[hep-ph\]](https://arxiv.org/abs/0802.1189).
- [28] M. Cacciari, G. P. Salam and G. Soyez, *FastJet user manual*, *Eur. Phys. J. C* **72** (2012) 1896, arXiv: [1111.6097 \[hep-ph\]](https://arxiv.org/abs/1111.6097).
- [29] ATLAS Collaboration, *Performance of pile-up mitigation techniques for jets in pp collisions at $\sqrt{s} = 8$ TeV using the ATLAS detector*, *Eur. Phys. J. C* **76** (2016) 581, arXiv: [1510.03823 \[hep-ex\]](https://arxiv.org/abs/1510.03823).
- [30] ATLAS Collaboration, *ATLAS b-jet identification performance and efficiency measurement with $t\bar{t}$ events in pp collisions at $\sqrt{s} = 13$ TeV*, *Eur. Phys. J. C* **79** (2019) 970, arXiv: [1907.05120 \[hep-ex\]](https://arxiv.org/abs/1907.05120).
- [31] ATLAS Collaboration, *Calibration of light-flavour b-jet mistagging rates using ATLAS proton–proton collision data at $\sqrt{s} = 13$ TeV*, ATLAS-CONF-2018-006, 2018, URL: <https://cds.cern.ch/record/2314418>.

[32] ATLAS Collaboration, *ATLAS flavour-tagging algorithms for the LHC Run 2 pp collision dataset*, (2022), arXiv: [2211.16345 \[physics.data-an\]](https://arxiv.org/abs/2211.16345).

[33] ATLAS Collaboration, *Performance of missing transverse momentum reconstruction with the ATLAS detector using proton–proton collisions at $\sqrt{s} = 13\text{ TeV}$* , *Eur. Phys. J. C* **78** (2018) 903, arXiv: [1802.08168 \[hep-ex\]](https://arxiv.org/abs/1802.08168).

[34] S. Frixione, *Isolated photons in perturbative QCD*, *Phys. Lett. B* **429** (1998) 369, arXiv: [hep-ph/9801442](https://arxiv.org/abs/hep-ph/9801442).

[35] D. Pagani, H.-S. Shao, I. Tsinikos and M. Zaro, *Automated EW corrections with isolated photons: $t\bar{t}\gamma$, $t\bar{t}\gamma\gamma$ and $t\gamma j$ as case studies*, *JHEP* **09** (2021) 155, arXiv: [2106.02059 \[hep-ph\]](https://arxiv.org/abs/2106.02059).

[36] J. Alwall et al., *The automated computation of tree-level and next-to-leading order differential cross sections, and their matching to parton shower simulations*, *JHEP* **07** (2014) 079, arXiv: [1405.0301 \[hep-ph\]](https://arxiv.org/abs/1405.0301).

[37] D. Pagani, I. Tsinikos and E. Vryonidou, *NLO QCD+EW predictions for tHj and tZj production at the LHC*, *JHEP* **08** (2020) 082, arXiv: [2006.10086 \[hep-ph\]](https://arxiv.org/abs/2006.10086).

[38] M. Cacciari, G. P. Salam and G. Soyez, *The catchment area of jets*, *JHEP* **04** (2008) 005, arXiv: [0802.1188 \[hep-ph\]](https://arxiv.org/abs/0802.1188).

[39] GEANT4 Collaboration, S. Agostinelli et al., *GEANT4 – a simulation toolkit*, *Nucl. Instrum. Meth. A* **506** (2003) 250.

[40] ATLAS Collaboration, *The ATLAS Simulation Infrastructure*, *Eur. Phys. J. C* **70** (2010) 823, arXiv: [1005.4568 \[physics.ins-det\]](https://arxiv.org/abs/1005.4568).

[41] ATLAS Collaboration, *Jet energy scale and resolution measured in proton–proton collisions at $\sqrt{s} = 13\text{ TeV}$ with the ATLAS detector*, *Eur. Phys. J. C* **81** (2020) 689, arXiv: [2007.02645 \[hep-ex\]](https://arxiv.org/abs/2007.02645).

[42] R. D. Ball et al., *Parton distributions for the LHC run II*, *JHEP* **04** (2015) 040, arXiv: [1410.8849 \[hep-ph\]](https://arxiv.org/abs/1410.8849).

[43] P. Artoisenet, R. Frederix, O. Mattelaer and R. Rietkerk, *Automatic spin-entangled decays of heavy resonances in Monte Carlo simulations*, *JHEP* **03** (2013) 015, arXiv: [1212.3460 \[hep-ph\]](https://arxiv.org/abs/1212.3460).

[44] T. Sjöstrand et al., *An introduction to PYTHIA 8.2*, *Comput. Phys. Commun.* **191** (2015) 159, arXiv: [1410.3012 \[hep-ph\]](https://arxiv.org/abs/1410.3012).

[45] R. D. Ball et al., *Parton distributions with LHC data*, *Nucl. Phys. B* **867** (2013) 244, arXiv: [1207.1303 \[hep-ph\]](https://arxiv.org/abs/1207.1303).

[46] ATLAS Collaboration, *ATLAS Pythia 8 tunes to 7 TeV data*, ATL-PHYS-PUB-2014-021, 2014, URL: <https://cds.cern.ch/record/1966419>.

[47] D. J. Lange, *The EvtGen particle decay simulation package*, *Nucl. Instrum. Meth. A* **462** (2001) 152.

[48] R. Frederix, E. Re and P. Torrielli, *Single-top t-channel hadroproduction in the four-flavour scheme with POWHEG and aMC@NLO*, *JHEP* **09** (2012) 130, arXiv: [1207.5391 \[hep-ph\]](https://arxiv.org/abs/1207.5391).

[49] P. Kant et al., *HatHor for single top-quark production: Updated predictions and uncertainty estimates for single top-quark production in hadronic collisions*, *Comput. Phys. Commun.* **191** (2015) 74, arXiv: [1406.4403 \[hep-ph\]](https://arxiv.org/abs/1406.4403).

[50] M. Aliev et al., *HATHOR – HAdronic Top and Heavy quarks crOss section calculatoR*, *Comput. Phys. Commun.* **182** (2011) 1034, arXiv: [1007.1327 \[hep-ph\]](https://arxiv.org/abs/1007.1327).

[51] D0 Collaboration, *Measurement of the $t\bar{t}$ production cross section in $p\bar{p}$ collisions at $\sqrt{s} = 1.96$ -TeV using kinematic characteristics of lepton + jets events*, *Phys. Rev. D* **76** (2007) 092007, arXiv: [0705.2788 \[hep-ex\]](https://arxiv.org/abs/0705.2788).

[52] ATLAS Collaboration, *Tools for estimating fake/non-prompt lepton backgrounds with the ATLAS detector at the LHC*, (2022), arXiv: [2211.16178 \[hep-ex\]](https://arxiv.org/abs/2211.16178).

[53] See Supplemental Material at [URL will be inserted by publisher] for technical descriptions of the estimation of the $e \rightarrow \gamma$ and $h \rightarrow \gamma$ backgrounds.

[54] CDF Collaboration, *Measurement of $\sigma B(W \rightarrow ev)$ and $\sigma B(Z^0 \rightarrow e^+e^-)$ in $\bar{p}p$ collisions at $\sqrt{s} = 1800$ GeV*, *Phys. Rev. D* **44** (1991) 29.

[55] ATLAS Collaboration, *Measurement of the photon identification efficiencies with the ATLAS detector using LHC Run 2 data collected in 2015 and 2016*, *Eur. Phys. J. C* **79** (2019) 205, arXiv: [1810.05087 \[hep-ex\]](https://arxiv.org/abs/1810.05087).

[56] ATLAS Collaboration, *Electron reconstruction and identification in the ATLAS experiment using the 2015 and 2016 LHC proton–proton collision data at $\sqrt{s} = 13$ TeV*, *Eur. Phys. J. C* **79** (2019) 639, arXiv: [1902.04655 \[hep-ex\]](https://arxiv.org/abs/1902.04655).

[57] ATLAS Collaboration, *Muon reconstruction performance of the ATLAS detector in proton–proton collision data at $\sqrt{s} = 13$ TeV*, *Eur. Phys. J. C* **76** (2016) 292, arXiv: [1603.05598 \[hep-ex\]](https://arxiv.org/abs/1603.05598).

[58] ATLAS Collaboration, *Jet energy scale measurements and their systematic uncertainties in proton–proton collisions at $\sqrt{s} = 13$ TeV with the ATLAS detector*, *Phys. Rev. D* **96** (2017) 072002, arXiv: [1703.09665 \[hep-ex\]](https://arxiv.org/abs/1703.09665).

[59] ATLAS Collaboration, *Measurement of b -tagging efficiency of c -jets in $t\bar{t}$ events using a likelihood approach with the ATLAS detector*, ATLAS-CONF-2018-001, 2018, URL: <https://cds.cern.ch/record/2306649>.

[60] F. Chollet et al., *Keras*, 2015, URL: <https://keras.io>.

[61] M. Abadi et al., *TensorFlow: Large-Scale Machine Learning on Heterogeneous Distributed Systems*, <https://www.tensorflow.org>, 2015.

[62] G. Cowan, K. Cranmer, E. Gross and O. Vitells, *Asymptotic formulae for likelihood-based tests of new physics*, *Eur. Phys. J. C* **71** (2011) 1554, arXiv: [1007.1727 \[physics.data-an\]](https://arxiv.org/abs/1007.1727), Erratum: *Eur. Phys. J. C* **73** (2013) 2501.

[63] R. J. Barlow and C. Beeston, *Fitting using finite Monte Carlo samples*, *Comput. Phys. Commun.* **77** (1993) 219.

[64] N. Kidonakis and N. Yamanaka, *QCD corrections in $tq\gamma$ production at hadron colliders*, *Eur. Phys. J. C* **82** (2022) 670, arXiv: [2201.12877 \[hep-ph\]](https://arxiv.org/abs/2201.12877).

[65] E. Bothmann et al., *Event generation with Sherpa 2.2*, *SciPost Phys.* **7** (2019) 034, arXiv: [1905.09127 \[hep-ph\]](#).

[66] T. Gleisberg and S. Höche, *Comix, a new matrix element generator*, *JHEP* **12** (2008) 039, arXiv: [0808.3674 \[hep-ph\]](#).

[67] S. Schumann and F. Krauss, *A parton shower algorithm based on Catani–Seymour dipole factorisation*, *JHEP* **03** (2008) 038, arXiv: [0709.1027 \[hep-ph\]](#).

[68] S. Höche, F. Krauss, M. Schönher and F. Siegert, *A critical appraisal of NLO+PS matching methods*, *JHEP* **09** (2012) 049, arXiv: [1111.1220 \[hep-ph\]](#).

[69] S. Höche, F. Krauss, M. Schönher and F. Siegert, *QCD matrix elements + parton showers. The NLO case*, *JHEP* **04** (2013) 027, arXiv: [1207.5030 \[hep-ph\]](#).

[70] S. Catani, F. Krauss, B. R. Webber and R. Kuhn, *QCD Matrix Elements + Parton Showers*, *JHEP* **11** (2001) 063, arXiv: [hep-ph/0109231](#).

[71] S. Höche, F. Krauss, S. Schumann and F. Siegert, *QCD matrix elements and truncated showers*, *JHEP* **05** (2009) 053, arXiv: [0903.1219 \[hep-ph\]](#).

[72] F. Buccioni et al., *OpenLoops 2*, *Eur. Phys. J. C* **79** (2019) 866, arXiv: [1907.13071 \[hep-ph\]](#).

[73] F. Cascioli, P. Maierhöfer and S. Pozzorini, *Scattering Amplitudes with Open Loops*, *Phys. Rev. Lett.* **108** (2012) 111601, arXiv: [1111.5206 \[hep-ph\]](#).

[74] F. Buccioni, S. Pozzorini and M. Zoller, *On-the-fly reduction of open loops*, *Eur. Phys. J. C* **78** (2018) 70, arXiv: [1710.11452 \[hep-ph\]](#).

[75] A. Denner, S. Dittmaier and L. Hofer, *COLLIER: A fortran-based complex one-loop library in extended regularizations*, *Comput. Phys. Commun.* **212** (2017) 220, arXiv: [1604.06792 \[hep-ph\]](#).

[76] S. Frixione, G. Ridolfi and P. Nason, *A positive-weight next-to-leading-order Monte Carlo for heavy flavour hadroproduction*, *JHEP* **09** (2007) 126, arXiv: [0707.3088 \[hep-ph\]](#).

[77] P. Nason, *A new method for combining NLO QCD with shower Monte Carlo algorithms*, *JHEP* **11** (2004) 040, arXiv: [hep-ph/0409146](#).

[78] S. Frixione, P. Nason and C. Oleari, *Matching NLO QCD computations with parton shower simulations: the POWHEG method*, *JHEP* **11** (2007) 070, arXiv: [0709.2092 \[hep-ph\]](#).

[79] S. Alioli, P. Nason, C. Oleari and E. Re, *A general framework for implementing NLO calculations in shower Monte Carlo programs: the POWHEG BOX*, *JHEP* **06** (2010) 043, arXiv: [1002.2581 \[hep-ph\]](#).

[80] S. Frixione, E. Laenen, P. Motylinski, C. White and B. R. Webber, *Single-top hadroproduction in association with a W boson*, *JHEP* **07** (2008) 029, arXiv: [0805.3067 \[hep-ph\]](#).

[81] M. Beneke, P. Falgari, S. Klein and C. Schwinn, *Hadronic top-quark pair production with NNLL threshold resummation*, *Nucl. Phys. B* **855** (2012) 695, arXiv: [1109.1536 \[hep-ph\]](#).

[82] M. Cacciari, M. Czakon, M. Mangano, A. Mitov and P. Nason, *Top-pair production at hadron colliders with next-to-next-to-leading logarithmic soft-gluon resummation*, *Phys. Lett. B* **710** (2012) 612, arXiv: [1111.5869 \[hep-ph\]](https://arxiv.org/abs/1111.5869).

[83] P. Bärnreuther, M. Czakon and A. Mitov, *Percent-Level-Precision Physics at the Tevatron: Next-to-Next-to-Leading Order QCD Corrections to $q\bar{q} \rightarrow t\bar{t} + X$* , *Phys. Rev. Lett.* **109** (2012) 132001, arXiv: [1204.5201 \[hep-ph\]](https://arxiv.org/abs/1204.5201).

[84] M. Czakon and A. Mitov, *NNLO corrections to top-pair production at hadron colliders: the all-fermionic scattering channels*, *JHEP* **12** (2012) 054, arXiv: [1207.0236 \[hep-ph\]](https://arxiv.org/abs/1207.0236).

[85] M. Czakon and A. Mitov, *NNLO corrections to top pair production at hadron colliders: the quark-gluon reaction*, *JHEP* **01** (2013) 080, arXiv: [1210.6832 \[hep-ph\]](https://arxiv.org/abs/1210.6832).

[86] M. Czakon, P. Fiedler and A. Mitov, *Total Top-Quark Pair-Production Cross Section at Hadron Colliders Through $O(\alpha_S^4)$* , *Phys. Rev. Lett.* **110** (2013) 252004, arXiv: [1303.6254 \[hep-ph\]](https://arxiv.org/abs/1303.6254).

[87] M. Czakon and A. Mitov, *Top++: A program for the calculation of the top-pair cross-section at hadron colliders*, *Comput. Phys. Commun.* **185** (2014) 2930, arXiv: [1112.5675 \[hep-ph\]](https://arxiv.org/abs/1112.5675).

[88] C. Anastasiou, L. Dixon, K. Melnikov and F. Petriello, *High-precision QCD at hadron colliders: Electroweak gauge boson rapidity distributions at next-to-next-to leading order*, *Phys. Rev. D* **69** (2004) 094008, arXiv: [hep-ph/0312266](https://arxiv.org/abs/hep-ph/0312266).

[89] N. Kidonakis, *Two-loop soft anomalous dimensions for single top quark associated production with a W^- or H^-* , *Phys. Rev. D* **82** (2010) 054018, arXiv: [1005.4451 \[hep-ph\]](https://arxiv.org/abs/1005.4451).

[90] K. Melnikov, M. Schulze and A. Scharf, *QCD corrections to top quark pair production in association with a photon at hadron colliders*, *Phys. Rev. D* **83** (2011) 074013, arXiv: [1102.1967 \[hep-ph\]](https://arxiv.org/abs/1102.1967).

[91] J. Butterworth et al., *PDF4LHC recommendations for LHC Run II*, *J. Phys. G* **43** (2016) 023001, arXiv: [1510.03865 \[hep-ph\]](https://arxiv.org/abs/1510.03865).

[92] A. D. Martin, W. J. Stirling, R. S. Thorne and G. Watt, *Uncertainties on α_S in global PDF analyses and implications for predicted hadronic cross sections*, *Eur. Phys. J. C* **64** (2009) 653, arXiv: [0905.3531 \[hep-ph\]](https://arxiv.org/abs/0905.3531).

[93] J. Gao et al., *CT10 next-to-next-to-leading order global analysis of QCD*, *Phys. Rev. D* **89** (2014) 033009, arXiv: [1302.6246 \[hep-ph\]](https://arxiv.org/abs/1302.6246).

[94] N. Kidonakis, *Next-to-next-to-leading-order collinear and soft gluon corrections for t-channel single top quark production*, *Phys. Rev. D* **83** (2011) 091503, arXiv: [1103.2792 \[hep-ph\]](https://arxiv.org/abs/1103.2792).

[95] N. Kidonakis, *Next-to-next-to-leading logarithm resummation for s-channel single top quark production*, *Phys. Rev. D* **81** (2010) 054028, arXiv: [1001.5034 \[hep-ph\]](https://arxiv.org/abs/1001.5034).

[96] ATLAS Collaboration, *Monte Carlo Generators for the Production of a W or Z/γ^* Boson in Association with Jets at ATLAS in Run 2*, ATL-PHYS-PUB-2016-003, 2016, URL: <https://cds.cern.ch/record/2120133>.

- [97] ATLAS Collaboration, *Measurements of inclusive and differential fiducial cross-sections of $t\bar{t}\gamma$ production in leptonic final states at $\sqrt{s} = 13$ TeV in ATLAS*, *Eur. Phys. J. C* **79** (2019) 382, arXiv: [1812.01697 \[hep-ex\]](https://arxiv.org/abs/1812.01697).
- [98] M. Bähr et al., *Herwig++ physics and manual*, *Eur. Phys. J. C* **58** (2008) 639, arXiv: [0803.0883 \[hep-ph\]](https://arxiv.org/abs/0803.0883).
- [99] J. Bellm et al., *Herwig 7.0/Herwig++ 3.0 release note*, *Eur. Phys. J. C* **76** (2016) 196, arXiv: [1512.01178 \[hep-ph\]](https://arxiv.org/abs/1512.01178).
- [100] ATLAS Collaboration,
Study of top-quark pair modelling and uncertainties using ATLAS measurements at $\sqrt{s} = 13$ TeV, ATL-PHYS-PUB-2020-023, 2020, URL: <https://cds.cern.ch/record/2730443>.